Two Finite-Element Discretizations for Gradient Elasticity

A. Zervos[1]; S.-A. Papanicolopulos[2]; and I. Vardoulakis, M.ASCE[3]

Abstract: We present and compare two different methods for numerically solving boundary value problems of gradient elasticity. The first method is based on a finite-element discretization using the displacement formulation, where elements that guarantee continuity of strains (i.e., C^1 interpolation) are needed. Two such elements are presented and shown to converge: a triangle with straight edges and an isoparametric quadrilateral. The second method is based on a finite-element discretization of Mindlin's elasticity with microstructure, of which gradient elasticity is a special case. Two isoparametric elements are presented, a triangle and a quadrilateral, interpolating the displacement and microdeformation fields. It is shown that, using an appropriate selection of material parameters, they can provide approximate solutions to boundary value problems of gradient elasticity. Benchmark problems are solved using both methods, to assess their relative merits and shortcomings in terms of accuracy, simplicity and computational efficiency. C^1 interpolation is shown to give generally superior results, although the approximate solutions obtained by elasticity with microstructure are also shown to be of very good quality.

DOI: 10.1061/(ASCE)0733-9399(2009)135:3(203)

CE Database subject headings: Finite element method; Elastic analysis; Microstructures; Numerical models.

Introduction

Conventional continuum descriptions and constitutive models used to describe the mechanical behavior of materials usually ignore the fact that materials have microstructure. The assumption used is that the dimensions of the modeled engineering structure (e.g., an embankment) are so much larger than the characteristic dimensions of the microstructure (e.g., the mean grain size of the soil), that the effect of the latter is insignificant. Nevertheless the above-mentioned assumption breaks down under certain conditions and microstructure dominates the macroscopic mechanical behavior. Conventional theories, like classical elastoplasticity, are then unable to reproduce the behavior observed. An example is localization of deformation in softening geomaterials, where the thickness of the localization bands is a function of the mean grain size (Mühlhaus and Vardoulakis 1987). Also, the existence of microstructure explains the scale effect observed in thick-cylinder tests of weak rocks (Papamichos and van den Hoek 1995; Papanastasiou and Vardoulakis 1989), or in metals (Fleck and Hutchinson 1997). To capture such phenomena, a model must incorporate length scales that correspond to the microstructural properties of the material modeled.

The first linear elastic constitutive model based on a continuum with microstructure was developed in Cosserat and Cosserat (1909), by introducing at each material point additional degrees of freedom of rotation. A more general framework was developed by Mindlin (1964) [and independently by Eringen and Suhubi (1964)], who postulated two distinct levels of deformation: one at the micro- and one at the macroscale. This theory assumed 12 independent degrees of freedom at each material point, namely three (macro-) displacements and 9 components of microdeformation. However, it is the special case of vanishing relative deformation, i.e., coincidence of the microdeformation with the displacement gradient, that has mostly attracted attention. In that special case, also known as gradient elasticity, the strain energy density becomes a function of the strains and the second derivatives of the displacement (Mindlin 1964; Mindlin and Eshel 1968; Toupin 1962). The extension of the previous ideas to plasticity started in the 1980s with the development of gradient plasticity theories (Aifantis 1984) and has continued since, attracting the interest of many authors (Vardoulakis and Frantziskonis 1992; de Borst and Mühlhaus 1992; Fleck and Hutchinson 1997; Ramaswamy and Aravas 1998; Zervos et al. 2001a, Voyiadjis and Abu Al-Rub 2005).

The numerical solution of boundary value problems of gradient elasticity, especially with the finite-element method, has been the subject of numerous research papers. A key difficulty is dealing with the higher-order terms that appear in the weak form, and different approaches for doing so have been proposed. Among them are mixed formulations (Amanatidou and Aravas 2002), meshless methods (Askes and Aifantis 2002), Lagrange multipliers (Shu et al. 1999; Matsushima et al. 2002), penalty methods (Zervos 2008), and other specialized numerical techniques (Askes and Gutierrez 2006). Employing the usual finite-element displacement formulation, where only the displacement field is discretized, has been consistently avoided despite being conceptually simpler. The reason is that it requires C^1-continuous interpolation, i.e., elements that guarantee continuity of strains. Such elements are perceived to be both difficult to implement and computationally expensive. Further, they are very few in number and they are currently restricted to one and two dimensions. However, the ex-

[1]Lecturer in Civil Engineering, School of Civil Engineering and the Environment, Univ. of Southampton, SO17 1BJ, U.K. E-mail: az@soton.ac.uk

[2]Doctoral Student, Section of Mechanics, National Technical Univ. of Athens, Zografou 157 73, Greece. E-mail: stefanos@mechan.ntua.gr

[3]Professor of Mechanics, Section of Mechanics, National Technical Univ. of Athens, Zografou 157 73, Greece. E-mail: I.Vardoulakis@mechan.ntua.gr

Note. Associate Editor: George Z. Voyiadjis. Discussion open until August 1, 2009. Separate discussions must be submitted for individual papers. The manuscript for this paper was submitted for review and possible publication on September 5, 2007; approved on October 15, 2008. This paper is part of the ***Journal of Engineering Mechanics***, Vol. 135, No. 3, March 1, 2009. ©ASCE, ISSN 0733-9399/2009/3-203–213/$25.00.

perience of successfully using C^1 interpolation in the context of gradient elastoplasticity (Zervos et al. 2001a, b, 2007, 2008) suggests that assessing the performance of such elements in the case of gradient elasticity, against one of the other approaches used, is a worthwhile exercise.

In this paper we present two different discretizations of gradient elasticity. One is based on the displacement formulation, requiring C^1 interpolation. Two different elements are examined, namely a triangle with straight edges and a mapped quadrilateral. The second discretization is based on the more general theory of elasticity with microstructure (Mindlin 1964) and employs a penalty approach to obtain solutions of gradient elasticity. Again two elements are examined, a triangle and a quadrilateral, both mapped. Comparisons between the results of the two methods are made, leading to an assessment of the respective rate of convergence of each element tested. The boundary value problems of simple shearing and of a thick-wall cylinder under external pressure are used as benchmarks. Based on the results, recommendations are made on the suitability of each element for the solution of general boundary value problems.

In the next section we summarize the basics of elasticity with microstructure and gradient elasticity. The different discretizations, the numerical solutions of benchmark problems and some comparisons of element performance are given in the following two sections. In the final section we draw some conclusions and provide recommendations.

Theoretical Background

For the sake of completeness the general framework of linear elasticity with microstructure is briefly presented in the first subsection here. Detailed derivations are skipped and the reader is referred to Mindlin (1964) for a detailed account. In the second subsection gradient elasticity is presented as a special case of this general framework. Tensor index notation is used throughout with the usual summation convention, and differentiation is signified by a comma between indices. Bracketed indices denote the antisymmetric part of the respective tensor and parenthesized ones denote the symmetric part.

Elasticity with Microstructure

We consider that each material particle is characterized by a position vector $\mathbf{x}_i$, it has a displacement vector $\mathbf{u}_i(\mathbf{x}_i)$ attached to it and also has a microvolume embedded in it. Within this microvolume, position is defined with respect to a new set of axes $\mathbf{x}_i'$, parallel to $\mathbf{x}_i$ and moving with the displacement $\mathbf{u}_i$, and the displacement within this microvolume is $\mathbf{u}_i'$. Microdeformation is then defined as $\boldsymbol{\psi}_{ij}=\mathbf{u}_{j,i'}'$, and can be split additively into microstrain $\boldsymbol{\psi}_{(ij)}$ and microrotation $\boldsymbol{\psi}_{[ij]}$. The strain and rotation tensors retain their usual definitions as the symmetric and antisymmetric parts respectively of the displacement gradient: $\boldsymbol{\epsilon}_{ij}=\boldsymbol{\epsilon}_{ji} \equiv (\mathbf{u}_{j,i}+\mathbf{u}_{i,j})/2$ and $\boldsymbol{\omega}_{ij}=-\boldsymbol{\omega}_{ji}\equiv(\mathbf{u}_{j,i}-\mathbf{u}_{i,j})/2$. The difference between the macro- and microdeformation is called the relative deformation: $\boldsymbol{\gamma}_{ij}\equiv\mathbf{u}_{j,i}-\boldsymbol{\psi}_{ij}$ and, finally, we define as microdeformation gradient the macrogradient of the microdeformation: $\boldsymbol{\kappa}_{ijk}\equiv\boldsymbol{\psi}_{jk,i}$. A schematic representation of the relations between different components of the kinematic quantities is given in Fig. 1.

For a centrosymmetric, isotropic material, the potential energy density and the constitutive relations linking stress-like quantities

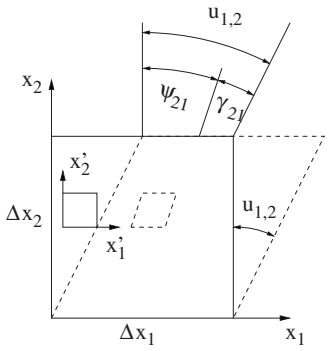

Fig. 1. Example of the relation between micro- and macrolevel kinematic quantities [adapted from Mindlin (1964)]; relation between $\partial u_1/\partial x_2$, ψ_{21}, and γ_{21}

to kinematic ones are written in terms of 18 independent material parameters $(\lambda,\mu,g_1,g_2,b_1,\ldots,b_3,a_1,\ldots,a_5,a_8,a_{10},a_{11},a_{13},\ldots,a_{15})$ (Mindlin 1964) as

$$\begin{aligned}W(\boldsymbol{\epsilon}_{ij},\boldsymbol{\gamma}_{ij},\boldsymbol{\kappa}_{ijk}) = {}& \tfrac{1}{2}\lambda\boldsymbol{\epsilon}_{ij}\boldsymbol{\epsilon}_{jj}+\mu\boldsymbol{\epsilon}_{ij}\boldsymbol{\epsilon}_{ij}+\tfrac{1}{2}b_1\boldsymbol{\gamma}_{ii}\boldsymbol{\gamma}_{jj}+\tfrac{1}{2}b_2\boldsymbol{\gamma}_{ij}\boldsymbol{\gamma}_{ij}\\ &+\tfrac{1}{2}b_3\boldsymbol{\gamma}_{ij}\boldsymbol{\gamma}_{ji}+g_1\boldsymbol{\gamma}_{ii}\boldsymbol{\epsilon}_{jj}+g_2(\boldsymbol{\gamma}_{ij}+\boldsymbol{\gamma}_{ji})\boldsymbol{\epsilon}_{ij}+a_1\boldsymbol{\kappa}_{iik}\boldsymbol{\kappa}_{kjj}\\ &+a_2\boldsymbol{\kappa}_{iik}\boldsymbol{\kappa}_{jkj}+\tfrac{1}{2}a_3\boldsymbol{\kappa}_{iik}\boldsymbol{\kappa}_{jjk}+\tfrac{1}{2}a_4\boldsymbol{\kappa}_{ijj}\boldsymbol{\kappa}_{ikk}+a_5\boldsymbol{\kappa}_{ijj}\boldsymbol{\kappa}_{kik}\\ &+\tfrac{1}{2}a_8\boldsymbol{\kappa}_{iji}\boldsymbol{\kappa}_{kjk}+\tfrac{1}{2}a_{10}\boldsymbol{\kappa}_{ijk}\boldsymbol{\kappa}_{ijk}+a_{11}\boldsymbol{\kappa}_{ijk}\boldsymbol{\kappa}_{jki}\\ &+\tfrac{1}{2}a_{13}\boldsymbol{\kappa}_{ijk}\boldsymbol{\kappa}_{ikj}+\tfrac{1}{2}a_{14}\boldsymbol{\kappa}_{ijk}\boldsymbol{\kappa}_{jik}+\tfrac{1}{2}a_{15}\boldsymbol{\kappa}_{ijk}\boldsymbol{\kappa}_{kji}\end{aligned} \tag{1}$$

$$\boldsymbol{\tau}_{ij}=\boldsymbol{\tau}_{ji}=\frac{\partial W}{\partial\boldsymbol{\epsilon}_{ij}}=\lambda\boldsymbol{\delta}_{ij}\boldsymbol{\epsilon}_{ll}+2\mu\boldsymbol{\epsilon}_{ij}+g_1\boldsymbol{\delta}_{ij}\boldsymbol{\gamma}_{ll}+g_2(\boldsymbol{\gamma}_{ij}+\boldsymbol{\gamma}_{ji}) \tag{2}$$

$$\boldsymbol{\sigma}_{ij}=\frac{\partial W}{\partial\boldsymbol{\gamma}_{ij}}=g_1\boldsymbol{\delta}_{ij}\boldsymbol{\epsilon}_{ll}+2g_2\boldsymbol{\epsilon}_{ij}+b_1\boldsymbol{\delta}_{ij}\boldsymbol{\gamma}_{ll}+b_2\boldsymbol{\gamma}_{ij}+b_3\boldsymbol{\gamma}_{ji} \tag{3}$$

$$\begin{aligned}\boldsymbol{\mu}_{ijk}=\frac{\partial W}{\partial\boldsymbol{\kappa}_{ijk}} = {}& a_1(\boldsymbol{\kappa}_{lli}\boldsymbol{\delta}_{jk}+\boldsymbol{\kappa}_{kll}\boldsymbol{\delta}_{ij})+a_2(\boldsymbol{\kappa}_{llj}\boldsymbol{\delta}_{ik}+\boldsymbol{\kappa}_{lkl}\boldsymbol{\delta}_{ij})+a_3\boldsymbol{\kappa}_{llk}\boldsymbol{\delta}_{ij}\\ &+a_4\boldsymbol{\kappa}_{ill}\boldsymbol{\delta}_{jk}+a_5(\boldsymbol{\kappa}_{jll}\boldsymbol{\delta}_{ik}+\boldsymbol{\kappa}_{lil}\boldsymbol{\delta}_{jk})+a_8\boldsymbol{\kappa}_{ljl}\boldsymbol{\delta}_{ik}+a_{10}\boldsymbol{\kappa}_{ijk}\\ &+a_{11}(\boldsymbol{\kappa}_{kij}+\boldsymbol{\kappa}_{jki})+a_{13}\boldsymbol{\kappa}_{ikj}+a_{14}\boldsymbol{\kappa}_{jik}+a_{15}\boldsymbol{\kappa}_{kji}\end{aligned} \tag{4}$$

In the previous equations, $\boldsymbol{\tau}_{ij}$=*Cauchy stress* and is energy conjugate to the strain; $\boldsymbol{\sigma}_{ij}$=*relative stress* energy conjugate to the relative deformation; and $\boldsymbol{\mu}_{ijk}$=*double stress* energy conjugate to the microdeformation gradient. In addition, four different types of external actions are considered: a body force $\mathbf{F}_i$ and a surface traction $\mathbf{t}_i$, which are energy conjugate to the displacement, and a body double-force $\boldsymbol{\Phi}_{ij}$ and surface double traction $\mathbf{T}_{ij}$, which are energy conjugate to the microdeformation. Equating the variation of total potential energy to the one of the work of external actions for independent variations of $\mathbf{u}_i$ and $\boldsymbol{\psi}_{ij}$, we recover the stress-type equations of motion and their boundary conditions (Mindlin 1964)

$$(\boldsymbol{\tau}_{ij}+\boldsymbol{\sigma}_{ij})_{,i}+\mathbf{F}_j=0 \tag{5}$$

$$\boldsymbol{\mu}_{ijk,i}+\boldsymbol{\sigma}_{jk}+\boldsymbol{\Phi}_{jk}=0 \tag{6}$$

$$\mathbf{t}_j=\mathbf{n}_i(\boldsymbol{\tau}_{ij}+\boldsymbol{\sigma}_{ij}) \tag{7}$$

$$\mathbf{T}_{jk} = \mathbf{n}_i \boldsymbol{\mu}_{ijk} \tag{8}$$

Conditions of plane strain exist if $u_3 = u'_{3'} = 0$ and $\partial(\cdot)/\partial x_3 = \partial(\cdot)/\partial x'_{3'} = 0$. Only six independent variables remain, namely u_1, u_2, ψ_{11}, ψ_{22}, ψ_{12}, and ψ_{21}. Such conditions are possible only if $a_1 = a_4 = a_5 = 0$ and $g_1 = b_1 = 0$ (Zervos 2008).

Overall, elasticity with microstructure provides a self-consistent theoretical framework for describing the mechanical behavior of elastic materials at different scales. There is a clear distinction between kinematic variables at the micro- and macroscales, and a clear physical interpretation for each one. Also, the way that the theory is constructed makes it a direct extension of classical elasticity, to which it reverts for vanishing microstructural parameters. A drawback, however, is the relatively large number of material parameters involved; 18 are needed even for the simple case of isotropic solids. This makes elasticity with microstructure difficult to calibrate: a large number of appropriate element tests would be required for fully characterizing a material, even if such stets can be devised. The much lower number of material parameters involved (i.e., 7) is one of the reasons why gradient elasticity, which is detailed in the following subsection, is widely preferred to the more general theory of elasticity with microstructure.

Gradient Elasticity as a Special Case

In the special case of vanishing relative deformation, $\boldsymbol{\gamma}_{ij} = 0 \Rightarrow \boldsymbol{\psi}_{ij} = \mathbf{u}_{j,i} \Rightarrow \boldsymbol{\kappa}_{ijk} = \mathbf{u}_{k,ij}$ and elasticity with microstructure degenerates to gradient elasticity. The potential energy density becomes $W = W(\boldsymbol{\epsilon}_{ij}, \mathbf{u}_{k,ij})$ or, equivalently, $W = \hat{W}(\boldsymbol{\epsilon}_{ij}, \hat{\boldsymbol{\kappa}}_{ijk} = \boldsymbol{\epsilon}_{jk,i})$ (Mindlin and Eshel 1968) and new stresses and double stresses can be defined as

$$\hat{W}(\boldsymbol{\epsilon}_{ij}, \hat{\boldsymbol{\kappa}}_{ijk}) = \tfrac{1}{2}\tilde{\lambda}\boldsymbol{\epsilon}_{ii}\boldsymbol{\epsilon}_{jj} + \tilde{\mu}\boldsymbol{\epsilon}_{ij}\boldsymbol{\epsilon}_{ij} + \hat{a}_1\hat{\boldsymbol{\kappa}}_{iik}\hat{\boldsymbol{\kappa}}_{kjj} + \hat{a}_2\hat{\boldsymbol{\kappa}}_{ijj}\hat{\boldsymbol{\kappa}}_{ikk} + \hat{a}_3\hat{\boldsymbol{\kappa}}_{ijk}\hat{\boldsymbol{\kappa}}_{jjk} + \hat{a}_4\hat{\boldsymbol{\kappa}}_{ijk}\hat{\boldsymbol{\kappa}}_{ijk} + \hat{a}_5\hat{\boldsymbol{\kappa}}_{ijk}\hat{\boldsymbol{\kappa}}_{kji} \tag{9}$$

$$\hat{\boldsymbol{\tau}}_{ij} = \hat{\boldsymbol{\tau}}_{ji} = \frac{\partial W}{\partial \boldsymbol{\epsilon}_{ij}} \tag{10}$$

$$\hat{\boldsymbol{\mu}}_{ijk} = \hat{\boldsymbol{\mu}}_{ikj} = \frac{\partial W}{\partial \hat{\boldsymbol{\kappa}}_{ijk}} \tag{11}$$

All the above-mentioned material parameters $(\tilde{\lambda}, \tilde{\mu}, \hat{a}_1, \ldots, \hat{a}_5)$ can be written in terms of the parameters λ, μ, b_i, g_i, and a_i used in the previous subsection (Mindlin and Eshel 1968).

The discussion on admissible boundary conditions in gradient elasticity and their relation to internal stress-like quantities is ongoing, and a reformulation of the relevant boundary value problem will be presented in a forthcoming paper (F. Froiio et al., personal communication, 2008). Here, three different types of external actions are considered: a body force $\mathbf{F}_i$ and a surface traction $\hat{\mathbf{P}}_i$, which are energy conjugate to the displacement, and a surface double-force $\hat{\mathbf{R}}_i$, which is energy conjugate to the normal derivative of the displacement at the boundary $D\mathbf{u}_i$. Equating the variation of total potential energy to the one of the work of external actions, for independent variations of $\mathbf{u}_i$ and $D\mathbf{u}_i$ we recover the respective stress-type equations of motion and their boundary conditions on smooth boundaries

$$(\hat{\boldsymbol{\tau}}_{jk} - \hat{\boldsymbol{\mu}}_{ijk,i})_{,j} + \mathbf{F}_j = 0 \tag{12}$$

$$\hat{\mathbf{P}}_k = \mathbf{n}_j(\hat{\boldsymbol{\tau}}_{jk} - \hat{\boldsymbol{\mu}}_{ijk,i}) - \mathbf{D}_j(\mathbf{n}_i\hat{\boldsymbol{\mu}}_{ijk}) + (\mathbf{D}_l\mathbf{n}_l)\mathbf{n}_i\mathbf{n}_j\hat{\boldsymbol{\mu}}_{ijk} \tag{13}$$

$$\hat{\mathbf{R}}_k = \mathbf{n}_i\mathbf{n}_j\hat{\boldsymbol{\mu}}_{ijk} \tag{14}$$

where $\mathbf{n}_i$ = outward normal to the boundary and $\mathbf{D_i}$ = surface gradient operator.

From the physical point of view, the relationship between elasticity with microstructure and gradient elasticity can be better appreciated through an analogy with the beam bending theories used in structural engineering. Elasticity with microstructure is analogous to the Timoshenko beam theory, as it employs two independent kinematic fields, namely the displacement $\mathbf{u}_i$ (analogous to the deflection of the beam w) and the microdeformation $\boldsymbol{\psi}_{ij}$ (analogous to cross-sectional rotation θ). Gradient elasticity on the other hand, where $\boldsymbol{\psi}_{ij} = \mathbf{u}_{j,i}$, is analogous to the Bernoulli–Euler beam theory, in which cross-sectional rotation equals the derivative of the deflection. The limiting case of $\boldsymbol{\gamma}_{ij} = 0$ is then analogous to the assumption of "infinite shear rigidity," which leads to the degeneration of the Timoshenko theory to the Bernoulli–Euler one.

Finite-Element Discretization of Gradient Elasticity

Direct Discretization

The simplest way of numerically treating the governing equations of gradient elasticity is by discretizing the equation of virtual work. Recalling Eqs. (10) and (11) and ignoring body forces for simplicity, this can be written as

$$\begin{aligned}\delta W_{\text{int}} &= \int_V (\hat{\boldsymbol{\tau}}_{ij}\delta\boldsymbol{\epsilon}_{ij} + \hat{\boldsymbol{\mu}}_{ijk}\delta\hat{\boldsymbol{\kappa}}_{ijk})dV \\ &= \int_V (\hat{\mathbf{P}}_k\delta\mathbf{u}_k + \hat{\mathbf{R}}_k\delta(D\mathbf{u}_k))dS \\ &= \delta W_{\text{ext}}\end{aligned} \tag{15}$$

Here we choose to discretize the displacement field $\mathbf{u}_i$ only. We write it in vector form as $\mathbf{u} = \mathbf{N}\cdot\hat{\mathbf{u}}$, where $\mathbf{N}$ = matrix of shape functions and $\hat{\mathbf{u}}$ are the degrees of freedom. All kinematic quantities can now be written in terms of $\hat{\mathbf{u}}$, the shape functions and their derivatives of appropriate order. The strain becomes $\boldsymbol{\epsilon} = \mathbf{B}_1\cdot\hat{\mathbf{u}}$ and the strain gradient $\boldsymbol{\kappa} = \mathbf{B}_2\cdot\hat{\mathbf{u}}$, where $\mathbf{B}_1$ and $\mathbf{B}_2$ contain first and second derivatives of $\mathbf{N}$, respectively. These are linked to the stress and the double stress through the constitutive relations, which can also be written in vector form. The stress becomes $\boldsymbol{\tau} = \mathbf{C}\cdot\boldsymbol{\epsilon}$ and the double stress $\boldsymbol{\mu} = \mathbf{D}\cdot\boldsymbol{\kappa}$, where $\mathbf{C}$ = usual elasticity matrix and $\mathbf{D}$ contains appropriate combinations of the material parameters $\hat{a}_i$. Substituting the previous equation into Eq. (15) yields the following stiffness equations:

$$\int_V (\mathbf{B}_1^T\mathbf{C}\mathbf{B}_1 + \mathbf{B}_2^T\mathbf{D}\mathbf{B}_2)dV\cdot\hat{\mathbf{u}} = \int_S (\mathbf{N}^T\cdot\mathbf{t})dS + \int_S \left(\frac{\partial}{\partial\mathbf{n}}\mathbf{N}^T\cdot\mathbf{T}\right)dS \rightarrow \mathbf{K}\cdot\hat{\mathbf{u}} = \mathbf{f} \tag{16}$$

where $\mathbf{K}$ = stiffness matrix and $\mathbf{f}$ = loading vector.

Due to the existence of strain gradients in the weak form, the interpolation used should guarantee continuity of strains. Here we will use two different plane C^1 elements. The first one (element Tri18) is the triangle shown in Fig. 2(a), which was originally presented in Argyris et al. (1968) and subsequently in Dasgupta and Sengupta (1990). The displacement is interpolated using a

J. Eng. Mech. 2009.135:203-213.

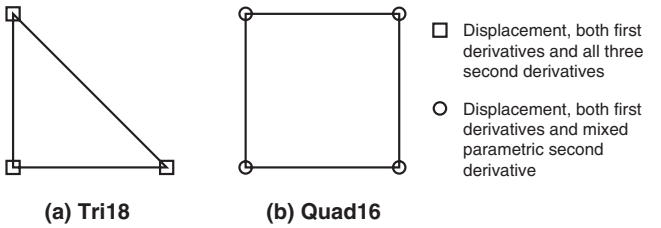

Fig. 2. Two elements that guarantee continuity of strains

quintic polynomial, whereas the normal derivative at the edges of the triangle is constrained to cubic. It has straight edges, uses only corner nodes, and it employs as degrees of freedom the displacement and all its derivatives of first and second order. For plane strain, this results to a total of 12 degrees of freedom per node, or 36 per element. The stiffness matrix is integrated using Gauss quadrature, with the 13-point scheme.

The second element we use (element Qad16) is the isoparametric quadrilateral shown in Fig. 2(b). It was first introduced for problems of fluid mechanics and plate bending by Petera and Pittman (1994) and employs cubic polynomials to interpolate the displacement. It has curved edges given by cubic splines, it uses only corner nodes, and it employs as degrees of freedom the displacement, the derivatives of first order and the mixed derivative of second order. The first-order derivatives used as degrees of freedom are derivatives taken with respect to the Cartesian coordinates. The mixed second-order derivative used as a degree of freedom is a derivative taken with respect to the reference coordinates ξ and η of the isoparametric formulation; it is not transformed into the Cartesian coordinate system. For plane strain this results to a total of 8 degrees of freedom per node, or 32 per element. The stiffness matrix is integrated using the 9-Gauss point scheme. The isoparametric formulation requires the calculation at the nodes of the derivatives of the Cartesian coordinates with respect to the parametric coordinates, which is performed as a preprocessing step; details of the relevant algorithms can be found in Petera and Pittman (1994). Due to its formulation, this element has the drawback that it can only be used in structured meshes.

The above-mentioned quadrilateral should not be confused with the rectangular element presented by Bogner et al. (1965), despite the fact that these two elements employ seemingly the same degrees of freedom. The latter is not a proper C^1 element, as it does not guarantee continuity of derivatives for arbitrary element orientations, whereas the quadrilateral of Petera and Pittman (1994) is based on a different philosophy and does not suffer from this drawback.

Discretization Based on a Penalty Constraint

An alternative discretization of gradient elasticity can be obtained through elasticity with Microstructure. Using Eqs. (2)–(4) and ignoring body forces, the principle of virtual work can be written as

$$\delta W_{\text{int}} = \int_V (\boldsymbol{\tau}_{ij}\delta\boldsymbol{\epsilon}_{ij} + \boldsymbol{\sigma}_{ij}\delta\boldsymbol{\gamma}_{ij} + \boldsymbol{\mu}_{ijk}\delta\boldsymbol{\kappa}_{ijk})dV$$
$$= \int_S (\mathbf{t}_i\delta\mathbf{u}_i + \mathbf{T}_{ij}\delta\boldsymbol{\psi}_{ij})dS$$
$$= \delta W_{\text{ext}} \tag{17}$$

We then consider an interpolation of $\mathbf{u}_i$ and $\boldsymbol{\psi}_{ij}$, written in vector form as $\mathbf{u}=\mathbf{N}_u\cdot\hat{\mathbf{u}}$ and $\boldsymbol{\psi}=\mathbf{N}_\psi\cdot\hat{\boldsymbol{\psi}}$, where $\mathbf{N}_u$ and $\mathbf{N}_\psi$=matrices of shape functions and $\hat{\mathbf{u}}$ and $\hat{\boldsymbol{\psi}}$ are the degrees of freedom. All kinematic quantities can be written in terms of $\hat{\mathbf{u}},\hat{\boldsymbol{\psi}}$, the shape functions and their derivatives of appropriate order. The deformation gradient becomes $\boldsymbol{\partial u}=\mathbf{B}_u\cdot\hat{\mathbf{u}}$, the rotation $\boldsymbol{\omega}=\mathbf{T}_a\cdot\mathbf{B}_u\cdot\hat{\mathbf{u}}$, the strain $\boldsymbol{\epsilon}=\mathbf{T}_s\cdot\mathbf{B}_u\cdot\hat{\mathbf{u}}$ and the relative deformation $\boldsymbol{\gamma}=\mathbf{B}_u\cdot\hat{\mathbf{u}}-\mathbf{N}_\psi\cdot\hat{\boldsymbol{\psi}}$. The matrix $\mathbf{B}_u$ contains first derivatives of $\mathbf{N}_u$, whereas matrices $\mathbf{T}_a$ and $\mathbf{T}_s$ simply rearrange the components of the displacement gradient to yield rotation and strain components, respectively. Finally, the microdeformation gradient is written in vector form as $\boldsymbol{\kappa}=\mathbf{B}_\psi\cdot\hat{\boldsymbol{\psi}}$, where the matrix $\mathbf{B}_\psi$ contains first derivatives of $\mathbf{N}_\psi$.

The constitutive relations can also be written in vector form. The Cauchy stress becomes $\boldsymbol{\tau}=\mathbf{C}\cdot\boldsymbol{\epsilon}+\mathbf{G}\cdot\mathbf{T}_s\cdot\gamma$, the relative stress $\boldsymbol{\sigma}=\mathbf{T}_s^T\cdot\mathbf{G}\cdot\boldsymbol{\epsilon}+\mathbf{B}\cdot\gamma$ and the double stress $\boldsymbol{\mu}=\mathbf{A}\cdot\boldsymbol{\kappa}$. The matrices $\mathbf{C}(\lambda,\mu)$, $\mathbf{G}(g_1,g_2)$, $\mathbf{B}(b_1,b_2,b_3)$, and $\mathbf{A}(a_i)$ introduced earlier contain appropriate combinations of the material parameters. Substituting the previous definitions into Eq. (17) and treating $\delta\hat{u}$ and $\delta\hat{\psi}$ as independent variations, we eventually arrive at the following set of stiffness equations:

$$\begin{bmatrix}\mathbf{K}_{uu} & \mathbf{K}_{u\psi}\\ \mathbf{K}_{\psi u} & \mathbf{K}_{\psi\psi}\end{bmatrix}\begin{Bmatrix}\hat{\mathbf{u}}\\ \hat{\boldsymbol{\psi}}\end{Bmatrix} = \begin{Bmatrix}\mathbf{f}_u\\ \mathbf{f}_\psi\end{Bmatrix} \rightarrow \mathbf{K}\cdot\hat{\mathbf{d}} = \mathbf{f} \tag{18}$$

where $\mathbf{K}$=overall stiffness matrix, which is symmetric as $\mathbf{K}_{\psi u}=\mathbf{K}_{u\psi}^T$. All integrations are carried out using Gauss quadrature and, for simplicity, all submatrices are integrated using the same scheme. For more detailed definitions of the vectors and matrices, the reader is referred to Zervos (2008). To demonstrate both the convergence of the formulation and the potential of elasticity with microstructure in simulating materials with multiscale behavior, a numerical example is presented in Appendix I.

We now recall from the previous section that gradient elasticity is a limiting case of elasticity with microstructure, for $\boldsymbol{\gamma}_{ij}=0$. For any gradient elastic solid, one could construct a corresponding solid obeying elasticity with microstructure, for which $\boldsymbol{\gamma}_{ij}\rightarrow 0$. Then the solution of any boundary value problem for the latter solid would be an approximate solution of the corresponding boundary value problem of gradient elasticity. The degree of approximation will depend on how small $\boldsymbol{\gamma}_{ij}$ is compared to other kinematic quantities. In this context, the discretization presented earlier can be seen as a discretization of gradient elasticity, provided an appropriate selection of parameters is made.

It is shown in Zervos (2008) that an appropriate selection of parameters is $g_1=g_2=b_1=b_3=a_1=a_4=a_5=a_{13}=a_{14}=a_{15}=0$, $\lambda=\tilde{\lambda}$, $\mu=\tilde{\mu}$, and

$$a_2=\frac{\hat{a}_1+\hat{a}_3}{2},\quad a_3=\frac{\hat{a}_3}{2},\quad a_8=\hat{a}_1+2\hat{a}_2+\frac{\hat{a}_3}{2},$$
$$a_{10}=\hat{a}_4+\frac{\hat{a}_5}{2},\quad a_{11}=\frac{\hat{a}_4}{2}+\frac{3\hat{a}_5}{4} \tag{19}$$

where $\tilde{\lambda}$, $\tilde{\mu}$ and $\hat{a}_1,\ldots,\hat{a}_5$=material parameters of the target gradient elastic solid. The only other parameter that needs to be defined is $b_2>0$. To impose the constraint $\boldsymbol{\gamma}_{ij}\rightarrow 0$, Eq. (1) suggests it must be $b_2\gg\{\lambda,\mu,a_2,a_3,a_8,a_{10},a_{11}\}$. The parameter b_2 is then interpreted as a penalty parameter whose value should be large enough to enforce the constraint to an acceptable approximation, but low enough to prevent ill-conditioning of the stiffness matrix. Experience shows that $10^2(\lambda+\mu)\leq b_2\leq 10^4(\lambda+\mu)$ suffices to obtain acceptable solutions.

J. Eng. Mech. 2009.135:203-213.

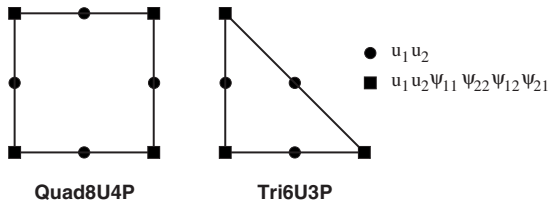

Fig. 3. Two elements that interpolate independently displacement and microdeformation

Standard C^0 discretization can be used to interpolate both $\mathbf{u}$ and $\boldsymbol{\psi}$, although certain combinations of shape functions will perform better than the others. It is worth investigating the properties that an interpolation should have so that it provides convergent results at the limit where $b_2 \to \infty$. It is shown in Appendix II that a necessary condition for convergence is

$$sN_{\mathrm{GP}} \geqslant n_{\boldsymbol{\psi}} \tag{20}$$

and a sufficient condition for convergence is

$$n_{\mathbf{u}} > n_{\boldsymbol{\psi}} + sN_{\mathrm{GP}} \quad \text{if} \quad n_{\boldsymbol{\psi}} \leqslant sN_{\mathrm{GP}} < n_{\mathbf{u}} \tag{21}$$

where n_u and n_ψ=number of degrees of freedom used for $\mathbf{u}$ and $\boldsymbol{\psi}$, respectively; N_{GP}=number of Gauss points integrating the stiffness; and s=number of the components of $\boldsymbol{\psi}$ entering the calculation [i.e., $s=4$ for two-dimensional (2D) problems and $s=9$ for three-dimensional ones]. The convergence of the penalty method has also been investigated by Mühlhaus et al. (2002) in the context of couple stress theory.

Here we choose to employ quadratic interpolation for $\mathbf{u}$ and linear interpolation for $\boldsymbol{\psi}$. This choice is motivated by the fact that $\boldsymbol{\psi}_{ij}$ is analogous to $\mathbf{u}_{i,j}$, so it is reasonable to use one order lower interpolation. In particular we use a six-node triangle (element Tri6U3P) and an eight-node quadrilateral (element Quad8U4P), both based on the respective isoparametric elements of the serendipity family; they are shown schematically in Fig. 3. The stiffness matrix is integrated using the 3-Gauss point scheme for the triangle and the 9-Gauss point scheme for the quadrilateral. It can be readily verified for both elements that they fulfill the above-mentioned necessary criterion for convergence. However, as this criterion is not also sufficient, convergence cannot be guaranteed a priori and is demonstrated in the following.

Numerical Results

In this section, both discretizations presented are used to solve boundary value problems and the performance of different elements is compared. The first subsection deals with shearing of an infinite layer and the second subsection with the problem of an elastic thick-wall cylinder. Both problems are solved using 2D elements and the results are discussed.

For simplicity we consider that, of all the material parameters appearing in Eq. (9), only the minimum number required for positive definiteness of the strain energy density have nonzero values. In particular we assume: $\tilde{\lambda}=7{,}000$, $\tilde{\mu}=3{,}000$, $\hat{\alpha}_1=\hat{\alpha}_3=\hat{\alpha}_5=0$, $\hat{\alpha}_2=\frac{1}{2}l^2\cdot\tilde{\lambda}$ and $\hat{\alpha}_4=l^2\cdot\tilde{\mu}$, where $l=0.01$ is an assumed internal length scale. According to the previous section and Eq. (19), the corresponding parameters of elasticity with microstructure are calculated as: $\lambda=7{,}000$, $\mu=3{,}000$, $a_2=a_3=0$, $a_8=l^2\lambda$, $a_{10}=l^2\mu$, $a_{11}=\frac{1}{2}l^2\mu$ and $g_1=g_2=b_1=b_3=a_1=a_4=a_5=a_{13}=a_{14}=a_{15}=0$. It is further assumed that the penalty parameter $b_2=1{,}000(\lambda+\mu)$.

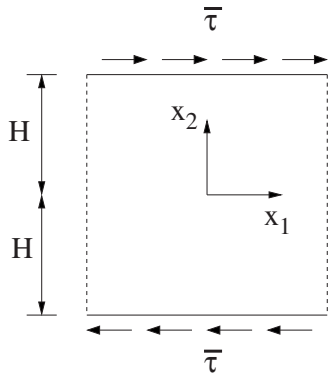

Fig. 4. Infinitely extending shear layer

Simple Shearing of an Infinite Layer

We consider the problem of simple shearing in plane strain of a layer $2H$ thick, extending infinitely in the lateral direction (Fig. 4). Only u_1 and $\partial u_1/\partial x_2$ are not identically zero, and the problem is one dimensional. The closed-form solution is derived in Appendix III.

The infinite layer will be modeled as a finite one with lateral extent $2L$; to eliminate boundary effects we set $L=50H$. The thickness of the layer is $2H=0.20$. Due to antisymmetry, only the top half of the layer needs to be considered. The bottom boundary of the model is fixed in both directions and the lateral boundaries are assumed free of constraints and double tractions. A uniform shear stress $\bar{\tau}$ is applied at the top boundary, where the boundary condition $\partial u_1/\partial x_2=0$ (i.e., "rough" boundary) is also assumed and $u_2=0$ is used to enforce simple shearing. The domain is subdivided into a uniform mesh having equal numbers of quadrilaterals along the length of the layer and along its thickness. The different meshes used have 4, 8, 12, 16, 32, 64, and 128 quadrilaterals along each direction, with each quadrilateral representing either a single element or, split along the diagonal, two triangular elements. Numerical results will be reported along the middle vertical line of the model, for different levels of mesh refinement. It is noted that strains are reported at the nodes using the values of corresponding degrees of freedom, rather than using extrapolated and averaged Gauss point values. Nodal values obtained thus were, in general, found to be more accurate, as they are direct results of the minimization process.

All elements capture the essence of the solution and give good quality results. As an example, Fig. 5 compares displacement and strain results for element Tri18 to the closed-form solution, for different levels of mesh refinement. The correct displacement and strain profiles, showing a clear boundary layer that covers about one quarter of the modelled thickness, are reproduced even for a coarse mesh. Elements Quad16, Tri6U3P, and Quad8U4P also give very good results. A first comparison is made in Fig. 6, where results of all four elements are plotted for an 8×8 mesh. The four results are all of good quality, to the extent that no clear conclusion can be drawn on the relative performance of the four elements from this plot.

A more direct comparison can be made by plotting the maximum error of each numerical solution versus the total number of degrees of freedom (DOFs) in the mesh, so that the rate of convergence of each element can also be appreciated. Displacement and strain errors are calculated as $\varepsilon_u=(u_{\mathrm{FE}}-u_0)/u_0$ and $\varepsilon_\epsilon=(\epsilon_{\mathrm{FE}}-\epsilon_0)/\epsilon_0$, respectively, where $(u_{\mathrm{FE}},\epsilon_{\mathrm{FE}})$ is the numerical solution and (u_0,ϵ_0) the closed-form one. The corresponding error

J. Eng. Mech. 2009.135:203-213.

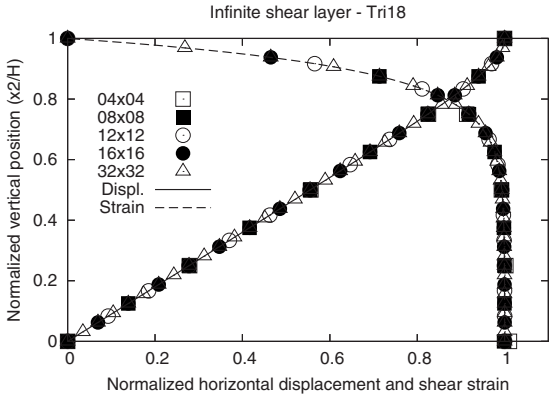

Fig. 5. Infinite shear layer: results for different meshes, element Tri18

plots for the displacement and strain profiles predicted by each element are shown in Fig. 7. Clearly, as the number of DOFs increases the maximum error decreases rapidly for all elements. Displacements are captured more accurately than strains in all cases, with a difference in maximum error of one to two orders of magnitude.

The penalty elements Tri6U3P and Quad8U4P give equally good results, reaching errors as low as 0.01% and showing a very good rate of convergence. Strain errors level off at about 0.1% and, although such a trend is not clear for displacement errors for

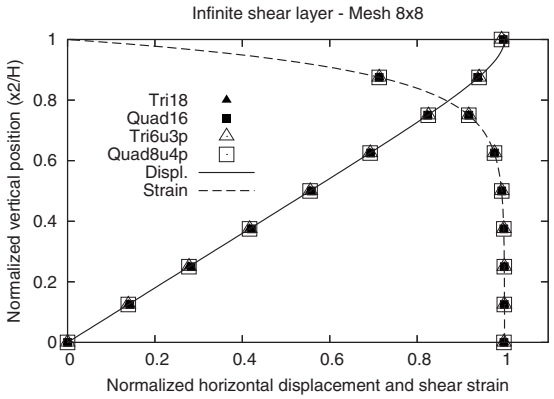

Fig. 6. Infinite shear layer: results for an 8×8 mesh and different elements

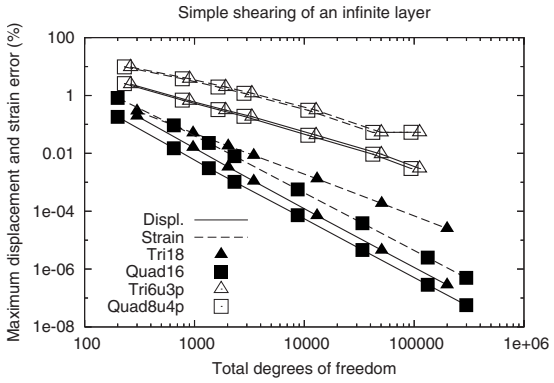

Fig. 7. Shear layer: maximum displacement and strain error vs mesh refinement

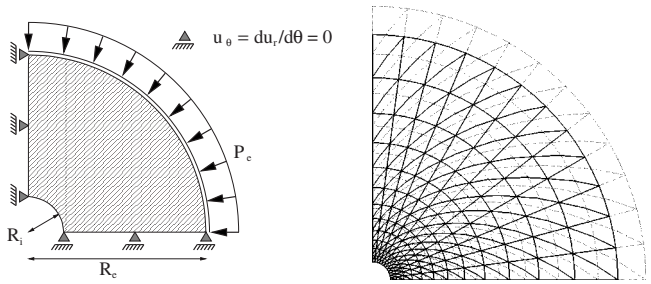

Fig. 8. Thick-wall cylinder problem: (a) geometry and boundary conditions and (b) the 12×12 mesh undeformed (dash line) and deformed (solid line)

the finest mesh used, it is expected that subsequent mesh refinement will be inefficient in proportionally improving accuracy. The existence of such a lower bound to errors is expected, given that the quality of the solution is influenced by the value of the penalty parameter b_2 as well as mesh density.

For the same number of DOFs the C^1 elements give superior results to those of the penalty elements, with at least one order of magnitude lower errors. Also, as evidenced by the steeper slope of the respective curves, C^1 elements converge faster. Comparing the position of the relevant data points in Fig. 7, we conclude that Tri18 meshes give equally good results with Quad16 meshes that have the same number of quadrilaterals in each direction, so from this point of view the two elements appear to be equivalent. Nevertheless, for the same mesh the total number of DOFs, and hence the computational cost, is lower if Quad16 is used, hence we conclude that Quad16 outperforms Tri18.

Thick-Wall Cylinder under External Pressure

We consider the problem of external pressurization of a thick-wall cylinder in plane strain. The internal and external radii of the cylinder are R_i and R_e, respectively, and the problem is axisymmetric. Due to the symmetries of the problem it suffices to consider the upper right quadrant of the geometry, shown in Fig. 8(a). The closed-form solution is derived in Appendix IV.

Here we assume $R_i=0.05$ and $R_e=0.50$. The internal boundary is traction-free, and a unit compressive radial stress $P_e=1.0$ is applied at the external one, as shown in Fig. 8(a). To guarantee that symmetry is preserved, appropriate boundary conditions must be applied at the bottom and left boundaries. Although in classical elasticity it suffices to prescribe zero displacement in the direction normal to these two boundaries, in gradient elasticity this is not sufficient, as the normal-to-the-boundary derivative of the displacement can be independently prescribed. Therefore, for the geometry of Fig. 8(a), the appropriate conditions are $u_\theta=u_y=0$ and $\partial u_r/\partial\theta=\partial u_x/\partial y=0$ at the bottom boundary, and $u_\theta=u_x=0$ and $\partial u_r/\partial\theta=\partial u_y/\partial x=0$ at the left boundary.

The domain is subdivided into a mesh having equal numbers of quadrilaterals along the radial and the tangential directions, using a geometric progression to produce a finer mesh near the hole. The different meshes used have 4, 8, 12, 16, 32, 64, and 128 quadrilaterals along each direction, with each quadrilateral representing either a single element or, split along the diagonal, two triangular elements. The ratio of the progression used for each mesh is $c=10^{1/N}$, where N=number of quadrilaterals in the radial direction. This choice of ratio guarantees that a $2N\times2N$ mesh is produced essentially by splitting into four each quadrilateral of an $N\times N$ mesh. The finer mesh then has a significant number of

J. Eng. Mech. 2009.135:203-213.

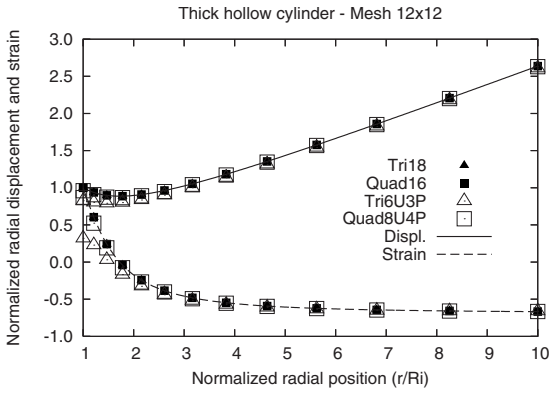

Fig. 9. Thick-wall cylinder: results for a 12×12 mesh and different elements

nodes in common with the coarser mesh, facilitating direct quantitative comparisons of nodal results. As an example of the meshes used, the 12×12 mesh is shown in Fig. 8(b). Numerical results will be reported along the 45° axis, for different levels of mesh refinement. Strains are again reported using nodal values of degrees of freedom.

As was the case with the shear layer, all elements can capture the essence of the solution and give good quality results. Fig. 9 compares radial displacement and strain results of all elements, for the 12×12 mesh. All elements can capture the far-field behavior, whereas C^1 elements appear to be better at capturing the solution near the hole.

A more detailed comparison can be made by plotting maximum error versus the total number of DOFs in the mesh. Displacement and strain errors are calculated as before, and the corresponding error plots are shown in Fig. 10. As expected, the maximum error decreases with increasing number of DOFs for all elements. Displacement errors are generally lower than strain errors, typically by one to two orders of magnitude.

The C^1 elements give clearly superior results compared to the penalty elements, and a better rate of convergence. The performance of Quad16 is particularly impressive compared to that of Tri18, as it consistently shows two orders of magnitude lower errors for the same number of DOFs. This is despite the fact that Tri18 employs a quintic polynomial, compared to the "bi-cubic"

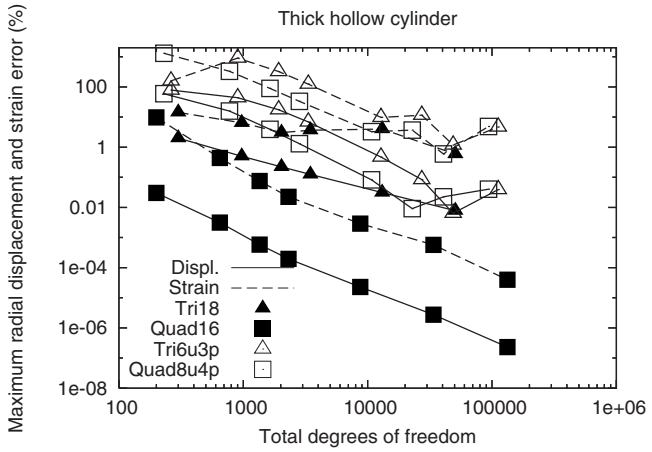

Fig. 10. Thick-wall cylinder: maximum radial displacement and strain error vs mesh refinement

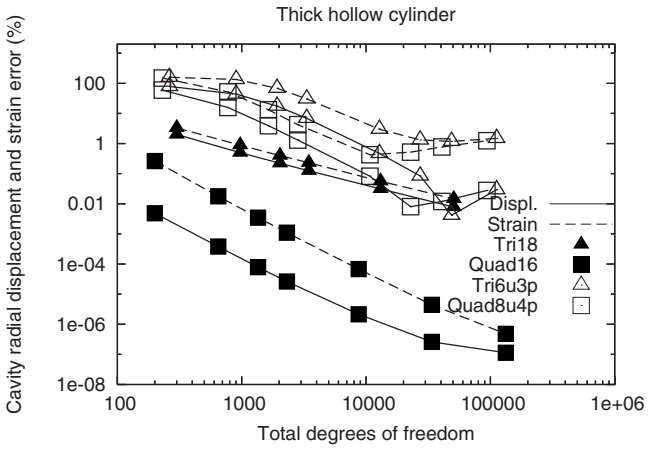

Fig. 11. Thick-wall cylinder: cavity radial displacement and strain error vs mesh refinement

employed by Quad16. The observed superiority of Quad16 is attributed to the fact that it is an isoparametric element, and therefore can model the geometry of the problem exactly. In contrast, Tri18 has straight edges and hence models the circular geometry as a polygonal one with reentrant or protruding corners. The error thus introduced decreases as the number of elements along the circumference of the cylinder increases, and Tri18 will give increasingly improving, convergent results as the mesh is refined. Its rate of convergence is, however, hampered by its straight edges; Quad16 gives better results for the same number of DOFs, and also a steeper slope in Fig. 10, meaning that it converges faster with mesh refinement.

The penalty elements Tri6U3P and Quad8U4P give good results, however their performance levels off at about 0.05% radial displacement error; this is again a result of the quality of the solution being influenced by the value of the penalty parameter b_2 as well as mesh density. What comes as a surprise in Fig. 10 is the magnitude of maximum strain errors, which does not appear to drop below 5% even for fine meshes. It was found that these significant errors occur at a radial distance $r/R_i \simeq 1.725$, where $\epsilon_{rr} \simeq 0$ (see Fig. 9), and are the result of division by near-zero reference values of ϵ_{rr} when calculating the error. Strain errors elsewhere in the model are typically one order of magnitude lower.

To appreciate better the performance of the penalty elements, the radial displacement and strain errors at the cavity wall ($r=R_i$) are plotted in Fig. 11. Fig. 11 confirms the results already reported earlier for the C^1 elements, although it is worth noting that they now appear to perform even better. Also, for both Tri6U3P and Quad8U4P the radial displacement and strain errors are now generally lower, with the former levelling off at about 0.03% and the latter at about 1%. These values are slightly higher than, but nevertheless compare well with, those achieved by the same elements for the shear layer problem, where the stress field is uniform. The corresponding approximate solutions can still be considered of very good quality.

Conclusions

In this paper we presented two different finite-element discretizations for gradient elasticity. The first one is based on the usual finite-element displacement formulation, and as a result it requires

J. Eng. Mech. 2009.135:203-213.

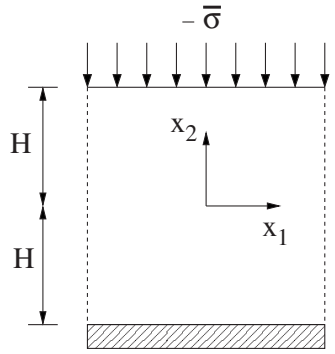

Fig. 12. 1D compression of a material layer

elements that guarantee C^1 continuity. Two such elements, a triangle with straight edges (Tri18) and an isoparametric quadrilateral (Quad16), were presented. The second discretization is based on a discretization of the more general theory of elasticity with microstructure, employing appropriate penalty constraints. Two relevant isoparametric elements were again presented, a triangle (Tri6U3P) and a quadrilateral (Quad8U4P).

The problems of an infinite shear layer and of a thick-wall cylinder under external pressure were solved as examples, and all four elements were shown to perform well. The penalty elements provided overall very good accuracy. As the quality of the solution obtained depends on the penalty parameter, as well as mesh density, there is a limit to the improvement in accuracy that can be obtained by mesh refinement for a given value of the penalty parameter. For the calculations presented, this minimum error for the displacement field was of the order of 0.05% or below and for the strain field 1% or below. These levels of approximation are considered satisfactory, and show that using the penalty approach with C^0 elements is a viable approach.

The C^1 elements, on the other hand, showed a robust performance, superior to that of the penalty elements. Quad16 outperformed Tri18 in terms of solution quality for the same number of DOFs. The difference is more marked if the domain has curved boundaries: then Tri18's rate of convergence is hampered by the element's straight edges, which can only approximately reproduce the geometry of the domain. Nevertheless, as Quad16 can only be used in structured meshses, Tri18 is the appropriate option for domains with complex geometry.

Acknowledgments

The first writer acknowledges the support of the School of Civil Engineering and the Environment, University of Southampton. The second writer acknowledges the support received through his scholarship from the Alexander S. Onassis Public Benefit Foundation. The third writer acknowledges the support of project Pythagoras, cofunded by the European Union (European Social Fund) and National Resources (EPEAEK II).

Appendix I. One-Dimensional Compression in Elasticity with Microstructure

As an example of modeling an elastic material with multiscale behavior, we use elasticity with microstructure to solve the problem of plane strain, one-dimensional (1D) compression of a material layer of finite thickness $2H$. The layer extends infinitely in the lateral direction (Fig. 12). Due to the geometry and type of loading, only u_2, ψ_{11}, and ψ_{22} are nonzero. We model the layer as having lateral extent $L=10H$, which suffices to eliminate boundary effects. Boundary conditions used are $u_2=0$ at $x_2=-H$ and $t_2=1.0$ at $x_2=H$. The lateral boundaries are horizontally constrained. In addition, we impose $\psi_{11}=\psi_{22}=\psi_{21}=\psi_{12}=0$ at $x_2=\pm H$, to simulate loading through fully rough contact.

The mesh used is uniform, consisting of 10×5 quadrilaterals. Each quadrilateral represents either a single Quad8U4P element or, split along the diagonal, two Tri6U3P elements. The material parameters used are $\lambda=b_2=7{,}000$, $\mu=b_3=g_2=3{,}000$, $a_{10}=7/10$ and $a_2=a_3=a_8=a_{11}=a_{13}=a_{14}=a_{15}=3/10$. Numerical results are reported along the middle vertical line of the model.

The vertical displacement u_2 and microdeformation ψ_{22}, normalized by their maximum value, are presented in Fig. 13(a). It can be readily seen that, although a linear displacement (i.e. constant strain) profile is evident in the middle of the layer, the simulations also predict the formation of a boundary layer close to the top and bottom boundaries. These boundary layers are due to the existence of microstructure, which leads to deformation taking place at more than one scale.

The effect of microstructure becomes more evident for different values of the material parameters a_i, which correspond to microstructural length scales. Fig. 13(b) shows results for the vertical strain profile for three cases, where the values of a_i are

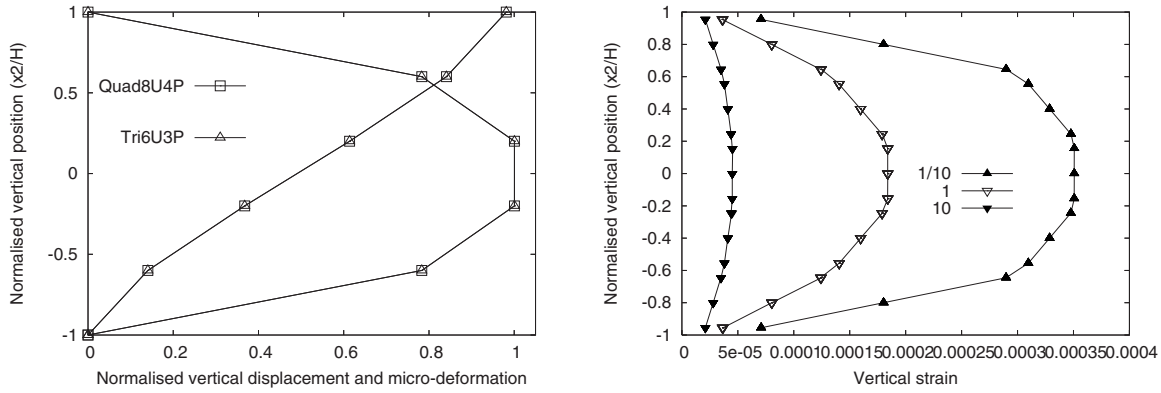

(a) u_2 and ψ_{22} profiles

(b) Vertical strain for different internal lengths

Fig. 13. Numerical results for 1D deformation of an elastic layer with microstructure

J. Eng. Mech. 2009.135:203-213.

varied by two orders of magnitude with all other parameters constant. It is clear that a scale effect is present, such that increasing the internal length scale increases the stiffness of the layer, whereas reducing it makes it more compliant. An equivalent statement would be that, for a given material, thinner layers are stiffer.

Appendix II. Necessary Conditions for Convergence of the Penalty Method

The stiffness equations of elasticity with microstructure are given in Eq. (18). For the particular choice of material parameters given in numerical results, and taking into account the matrix definitions detailed in Zervos (2008), these can be rewritten as

$$\left\{\begin{bmatrix}\mathbf{K}^{s}_{\mathbf{uu}} & 0\\ 0 & \mathbf{K}^{s}_{\boldsymbol{\psi}\boldsymbol{\psi}}\end{bmatrix}+b_2\cdot\begin{bmatrix}\mathbf{K}^{\mathbf{p}}_{\mathbf{uu}} & \mathbf{K}^{\mathbf{p}}_{\mathbf{u}\boldsymbol{\psi}}\\ \mathbf{K}^{\mathbf{p}}_{\boldsymbol{\psi}\mathbf{u}} & \mathbf{K}^{\mathbf{p}}_{\boldsymbol{\psi}\boldsymbol{\psi}}\end{bmatrix}\right\}\begin{Bmatrix}\hat{\mathbf{u}}\\ \hat{\boldsymbol{\psi}}\end{Bmatrix}=\begin{Bmatrix}\mathbf{f}_{\mathbf{u}}\\ \mathbf{f}_{\boldsymbol{\psi}}\end{Bmatrix} \tag{22}$$

where a superscript s denotes "normal" stiffness terms and a superscript p=stiffness terms corresponding to the penalty constraint. It is trivial to show that, at the limit $b_2\to\infty$, the abovementioned equation becomes

$$\begin{bmatrix}\mathbf{K}^{\mathbf{p}}_{\mathbf{uu}} & \mathbf{K}^{\mathbf{p}}_{\mathbf{u}\boldsymbol{\psi}}\\ \mathbf{K}^{\mathbf{p}}_{\boldsymbol{\psi}\mathbf{u}} & \mathbf{K}^{\mathbf{p}}_{\boldsymbol{\psi}\boldsymbol{\psi}}\end{bmatrix}\begin{Bmatrix}\hat{\mathbf{u}}\\ \hat{\boldsymbol{\psi}}\end{Bmatrix}=\begin{Bmatrix}0\\ 0\end{Bmatrix}\to\begin{Bmatrix}\hat{\boldsymbol{\psi}}=-(\mathbf{K}^{\mathbf{p}}_{\boldsymbol{\psi}\boldsymbol{\psi}})^{-1}\cdot\mathbf{K}^{\mathbf{p}}_{\boldsymbol{\psi}\mathbf{u}}\cdot\hat{\mathbf{u}}\\ [\mathbf{K}^{\mathbf{p}}_{\mathbf{uu}}-\mathbf{K}^{\mathbf{p}}_{\mathbf{u}\boldsymbol{\psi}}\cdot(\mathbf{K}^{\mathbf{p}}_{\boldsymbol{\psi}\boldsymbol{\psi}})^{-1}\cdot\mathbf{K}^{\mathbf{p}}_{\boldsymbol{\psi}\mathbf{u}}]\cdot\hat{\mathbf{u}}=0\end{Bmatrix} \tag{23}$$

where

$$\mathbf{K}^{\mathbf{p}}_{\mathbf{uu}}=\int_V\mathbf{B}^{\mathbf{T}}_{\mathbf{u}}\mathbf{B}_{\mathbf{u}}dV,\quad \mathbf{K}^{\mathbf{p}}_{\boldsymbol{\psi}\boldsymbol{\psi}}=\int_V\mathbf{N}^{\mathbf{T}}_{\boldsymbol{\psi}}\mathbf{N}_{\boldsymbol{\psi}}dV,$$

$$\mathbf{K}^{\mathbf{p}}_{\mathbf{u}\boldsymbol{\psi}}=(\mathbf{K}^{\mathbf{p}}_{\boldsymbol{\psi}\mathbf{u}})^{\mathbf{T}}=-\int_V\mathbf{B}^{\mathbf{T}}_{\mathbf{u}}\mathbf{N}_{\boldsymbol{\psi}}dV \tag{24}$$

with $\mathbf{N}_{\mathbf{u}}$ and $\mathbf{N}_{\boldsymbol{\psi}}$=shape functions used for $\mathbf{u}$ and $\boldsymbol{\psi}$, and $\mathbf{B}_u=\nabla\mathbf{N}_u$.

From Eq. (23) we determine directly that, for a nonzero solution to the stiffness equations to exist, matrix $\mathbf{K}^{p}_{\boldsymbol{\psi}\boldsymbol{\psi}}$ *must be nonsingular* and the matrix premultiplying $\hat{\mathbf{u}}$ in the second line *must be singular*. These conditions are necessary for convergence, so if either is violated locking will occur. However, they are not sufficient, and any element fulfilling them should also be tested numerically to prove convergence. In the following we elaborate these two conditions, denoting with $\mathbf{n}_u$ and $\mathbf{n}_{\boldsymbol{\psi}}$=numbers of degrees of freedom used for $\mathbf{u}$ and $\boldsymbol{\psi}$, respectively, with N_{GP}=number of Gauss points used and with s=number of the components of $\boldsymbol{\psi}$ entering the calculation (i.e., $s=4$ for 2D problems and $s=9$ for 3D ones).

$\mathbf{K}^{p}_{\boldsymbol{\psi}\boldsymbol{\psi}}$ is an $n_{\boldsymbol{\psi}}\times n_{\boldsymbol{\psi}}$ matrix approximated numerically, through Gauss quadrature, as the sum of N_{GP} matrices, each one the result of an $(n_{\boldsymbol{\psi}}\times s)\times(s\times n_{\boldsymbol{\psi}})$ multiplication [c.f. Eq. (24)]. Clearly, rank $\mathbf{K}^{p}_{\boldsymbol{\psi}\boldsymbol{\psi}}\leqslant sN_{\mathrm{GP}}$, so the matrix may be nonsingular (i.e., have rank $n_{\boldsymbol{\psi}}$) only if

$$sN_{\mathrm{GP}}\geqslant n_{\boldsymbol{\psi}} \tag{25}$$

which is a necessary condition for convergence.

Similarly, $\mathbf{K}^{p}_{u\boldsymbol{\psi}}=(\mathbf{K}^{p}_{\boldsymbol{\psi}u})^{T}$ is an $n_u\times n_{\boldsymbol{\psi}}$ matrix approximated numerically as the sum of N_{GP} matrices, each one the result of an $(n_u\times s)\times(s\times n_{\boldsymbol{\psi}})$ multiplication [c.f. Eq. (24)]. Therefore, rank $\mathbf{K}^{p}_{u\boldsymbol{\psi}}\leqslant\min\{n_u,n_{\boldsymbol{\psi}},sN_{\mathrm{GP}}\}$. Following a similar argument, rank $\mathbf{K}^{p}_{uu}\leqslant\min\{n_u,sN_{\mathrm{GP}}\}$. Then, in view also of Eq. (25):

$$\mathrm{rank}[\mathbf{K}^{\mathbf{p}}_{\mathbf{u}\dot{\mathbf{u}}}-\mathbf{K}^{\mathbf{p}}_{\mathbf{u}\boldsymbol{\psi}}\cdot(\mathbf{K}^{\mathbf{p}}_{\boldsymbol{\psi}\boldsymbol{\psi}})^{-1}\cdot\mathbf{K}^{\mathbf{p}}_{\boldsymbol{\psi}\mathbf{u}}]\leqslant\min\{n_u,sN_{\mathrm{GP}}\}+\min\{n_u,n_{\boldsymbol{\psi}}\}. \tag{26}$$

The matrix on the left-hand side must be singular, i.e., have rank less than n_u. If $n_u\leqslant n_{\boldsymbol{\psi}}\leqslant sN_{\mathrm{GP}}$ or $n_{\boldsymbol{\psi}}<n_u\leqslant sN_{\mathrm{GP}}$ no useful constraint can be established from the previous equation, and singularity must be tested numerically. If $n_{\boldsymbol{\psi}}\leqslant sN_{\mathrm{GP}}<n_u$, however, the matrix will certainly be singular if $n_u>n_{\boldsymbol{\psi}}+s\cdot N_{\mathrm{GP}}$. The combination of the last two inequalities amounts to a sufficient condition for convergence, although not a necessary one.

Appendix III. Gradient Elasticity Solution for a Shear Layer

We consider the problem of Fig. 4. As only u_1 and $\partial u_1/\partial x_2$ are not identically zero, the problem is one-dimensional. From Eqs. (10)–(12) we obtain the following governing equation, where a prime denotes differentiation with respect to x_2:

$$\left(\frac{\hat{\alpha}_3}{2}+\hat{\alpha}_4+\frac{\hat{\alpha}_5}{2}\right)u_1''''-\tilde{\mu}u_1''=0 \tag{27}$$

The general solution is

$$u_1=C_1+C_2x_2+C_3\sinh\left(\frac{x_2}{\hat{l}}\right)+C_4\cosh\left(\frac{x_2}{\hat{l}}\right)$$

$$\hat{l}=\sqrt{\frac{1}{\tilde{\mu}}\left(\frac{\hat{\alpha}_3}{2}+\hat{\alpha}_4+\frac{\hat{\alpha}_5}{2}\right)} \tag{28}$$

where C_1–C_4=integration constants. Considering the boundary conditions $u_1(0)=0$, $\partial u_1/\partial x_2(\pm H)=0$, and $\hat{P}_1(\pm H)=\pm\bar{\tau}$ [see Eq. (12)], where $\bar{\tau}$=applied shear stress, we eventually obtain

$$u_1=\frac{\bar{\tau}}{\tilde{\mu}}\left[x_2-\hat{l}\cdot\frac{\sinh(x_2/\hat{l})}{\cosh(H/\hat{l})}\right] \tag{29}$$

$$\gamma_{12}=u_1'=\frac{\bar{\tau}}{\tilde{\mu}}\left[1-\frac{\cosh(x_2/\hat{l})}{\cosh(H/\hat{l})}\right] \tag{30}$$

We observe that, away from the top boundary, the displacement and strain fields are equal to the ones predicted by classical elasticity. Close to the applied shear stress, however, a boundary layer forms due to the interaction assumed between the gradient elastic body and the loading agent. The solution of classical elasticity is recovered for $\hat{l}=0$.

Appendix IV. Gradient Elasticity Solution for a Thick-Hollow Cylinder

We consider the problem of Fig. 8. Using polar coordinates r and θ, the only displacement component that is not identically zero is $u_\tau(r)$. Rewriting Eqs. (9)–(14) using covariant and contravariant indices and using covariant differentiation, we obtain the following governing equation, where a prime denotes differentiation with respect to r:

J. Eng. Mech. 2009.135:203-213.

$$2(\hat{\alpha}_1+\hat{\alpha}_2+\hat{\alpha}_3+\hat{\alpha}_4+\hat{\alpha}_5)\left(u_r''''+\frac{2u_r'''}{r}-\frac{3u_r''}{r^2}+\frac{3u_r'}{r^3}-\frac{3u_r}{r^4}\right)$$

$$-(\tilde{\lambda}+2\tilde{\mu})\left(u_r''+\frac{u_r'}{r}-\frac{u_r}{r^2}\right)=0 \tag{31}$$

The general solution is

$$u_r = C_1 r + \frac{C_2\hat{l}^2}{r} + C_3\hat{l}I_1\left(\frac{r}{\hat{l}}\right) + C_4\hat{l}K_1\left(\frac{r}{\hat{l}}\right)$$

$$\hat{l} = \sqrt{\frac{2(\hat{\alpha}_1+\hat{\alpha}_2+\hat{\alpha}_3+\hat{\alpha}_4+\hat{\alpha}_5)}{\tilde{\lambda}+2\tilde{\mu}}} \tag{32}$$

where C_1-C_4=dimensionless integration constants and I_1, K_1=modified Bessel functions of the first and second kind, respectively.

Setting $\rho=r/\hat{l}$ we get

$$u_r = \hat{l}\left(C_1\rho+\frac{C_2}{\rho}+C_3I_1(\rho)+C_4K_1(\rho)\right) \tag{33}$$

$$\epsilon_{rr} = C_1-\frac{C_2}{\rho^2}-C_3\left(\frac{I_1(\rho)}{\rho}-I_0(\rho)\right)-C_4\left(\frac{K_1(\rho)}{\rho}+K_0(\rho)\right) \tag{34}$$

The values of the integration constants are derived considering the boundary conditions for the surface tractions and double forces at the internal boundary $\rho=\alpha$ and the external boundary $\rho=\beta$

$$\hat{P}_{r|\alpha}=0,\quad \hat{P}_{r|\beta}=p,\quad \hat{R}_{r|\alpha}=0,\quad \hat{R}_{r|\beta}=0 \tag{35}$$

The integration constants are given by

$$C_1 = \frac{p}{2(\tilde{\lambda}+\tilde{\mu})}\frac{1}{\chi}\left(\frac{1}{\zeta\alpha^2}(\phi_\alpha\psi_\beta-\phi_\beta\psi_\alpha)+\frac{I_1(\alpha)}{\alpha}(\psi_\beta-\psi_\alpha)-\frac{K_1(\alpha)}{\alpha}(\phi_\beta-\phi_\alpha)\right)$$

$$C_2 = \frac{p}{2(\tilde{\lambda}+\tilde{\mu})}\frac{\phi_\alpha\psi_\beta-\phi_\beta\psi_\alpha}{\chi}$$

$$C_3 = \frac{p}{2(\tilde{\lambda}+\tilde{\mu})}\frac{-(\psi_\beta-\psi_\alpha)}{\chi}$$

$$C_4 = \frac{p}{2(\tilde{\lambda}+\tilde{\mu})}\frac{\phi_\beta-\phi_\alpha}{\chi} \tag{36}$$

where the expressions given below have been introduced for clarity

$$\xi=\frac{\hat{\alpha}_1+\hat{\alpha}_2+\hat{\alpha}_3+\hat{\alpha}_4+\hat{\alpha}_5}{2(\hat{\alpha}_4+\hat{\alpha}_5)},\quad \zeta=\frac{\tilde{\lambda}+\tilde{\mu}}{\tilde{\mu}} \tag{37}$$

$$\phi_\alpha=(\alpha^3\xi+\alpha)I_1(\alpha)-\frac{\alpha^2}{2}I_0(\alpha)$$

$$\psi_\alpha=(\alpha^3\xi+\alpha)K_1(\alpha)+\frac{\alpha^2}{2}K_0(\alpha)$$

$$\phi_\beta=(\beta^3\xi+\beta)I_1(\beta)-\frac{\beta^2}{2}I_0(\beta)$$

$$\psi_\beta=(\beta^3\xi+\beta)K_1(\beta)+\frac{\beta^2}{2}K_0(\beta) \tag{38}$$

$$\chi=-\frac{1}{\zeta}\left(\frac{1}{\beta^2}-\frac{1}{\alpha^2}\right)(\phi_\alpha\psi_\beta-\phi_\beta\psi_\alpha)-\left(\frac{I_1(\beta)}{\beta}-\frac{I_1(\alpha)}{\alpha}\right)(\psi_\beta-\psi_\alpha)+\left(\frac{K_1(\beta)}{\beta}-\frac{K_1(\alpha)}{\alpha}\right)(\phi_\beta-\phi_\alpha) \tag{39}$$

References

Aifantis, E. (1984). "On the microstructural origin of certain inelastic models." *J. Eng. Mater. Technol.*, 106(4), 326–330.

Amanatidou, E., and Aravas, N. (2002). "Mixed finite element formulations of strain-gradient elasticity problems." *Comput. Methods Appl. Mech. Eng.*, 191(15), 1723–1751.

Argyris, J. H., Fried, I., and Scharpf, D. W. (1968). "The tuba family of plate elements for the matrix displacement method." *Aeronaut. J.*, 72, 701–709.

Askes, H., and Aifantis, E. C. (2002). "Numerical modelling of size effects with gradient elasticity—Formulation, meshless discretization and examples." *Int. J. Fract.*, 117(4), 347–358.

Askes, H., and Gutierrez, M. (2006). "Implicit gradient elasticity." *Int. J. Numer. Methods Eng.*, 67(3), 400–416.

Bogner, F. K., Fox, R. L., and Schmit, L. A. (1965). "The generation of inter-element-compatible stiffness and mass matrices by the use of interpolation formulas." *Proc., Conf. on Matrix Methods in Structural Mechanics*, Air Force Institute of Technology, Wright-Patterson AF Base, Ohio, 397–443.

Cosserat, E., and Cosserat, F. (1909). *Théorie des corps déformables*, A. Hermann, Paris.

Dasgupta, S., and Sengupta, D. (1990). "A higher-order triangular plate bending element revisited." *Int. J. Numer. Methods Eng.*, 30(3), 419–430.

de Borst, R., and Mühlhaus, H.-B. (1992). "Gradient-dependent plasticity: formulation and algorithmic aspects." *Int. J. Numer. Methods Eng.*, 35(3), 521–539.

Eringen, A. C., and Suhubi, E. S. (1964). "Nonlinear theory of simple microelastic solid—I." *Int. J. Eng. Sci.*, 2(2), 189–203.

Fleck, N. A., and Hutchinson, J. W. (1997). "Strain gradient plasticity." *Advances in applied mechanics—33*, E. van derGiessen, T. Wu, and H. Aref, eds., Elsevier, Amsterdam, The Netherlands, 295–361.

Matsushima, T., Chambon, R., and Caillerie, D. (2002). "Large strain finite element analysis of a local second gradient model: Application to localization." *Int. J. Numer. Methods Eng.*, 54(4), 499–521.

Mindlin, R. (1964). "Microstructure in linear elasticity." *Arch. Ration. Mech. Anal.*, 16(1), 51–78.

Mindlin, R., and Eshel, N. N. (1968). "On first strain-gradient theories in linear elasticity." *Int. J. Solids Struct.*, 4(1), 109–124.

Mühlhaus, H.-B., Dufour, F., Moresi, L., and Hobbs, B. (2002). "A director theory for visco-elastic folding instabilities in multilayered rock." *Int. J. Solids Struct.*, 39(13), 3675–3691.

Mühlhaus, H.-B., and Vardoulakis, I. (1987). "The thickness of shear bands in granular materials." *Geotechnique*, 37(3), 271–283.

Papamichos, E., and van den Hoek, P. (1995). "Size dependency of castlegate and berea sandstone hollow-cylinder strength on the basis of bifurcation theory." *Proc., 35th U.S. Symp. on Rock Mechanics*, Taylor & Francis, Reno, Nev., 301–306.

Papanastasiou, P., and Vardoulakis, I. (1989). "Bifurcation analysis of deep boreholes. II: scale effect." *Int. J. Numer. Analyt. Meth. Geomech.*, 13(2), 183–198.

Petera, J., and Pittman, J. (1994). "Isoparametric hermite elements." *Int. J. Numer. Methods Eng.*, 37(20), 3489–3519.
Ramaswamy, S., and Aravas, N. (1998). "Finite element implementation of gradient plasticity models. Part I: Gradient-dependent yield functions." *Comput. Methods Appl. Mech. Eng.*, 163(1–4), 11–32.
Shu, J. Y., King, W. E., and Fleck, N. A. (1999). "Finite elements for materials with strain gradient effects." *Int. J. Numer. Methods Eng.*, 44(3), 373–391.
Toupin, R. (1962). "Elastic materials with couple stresses." *Arch. Ration. Mech. Anal.*, 11(1), 385–414.
Vardoulakis, I., and Frantziskonis, G. (1992). "Micro-structure in kinematic-hardening plasticity." *Eur. J. Mech. A/Solids*, 11(4), 467–486.
Voyiadjis, G., and Abu Al-Rub, R. (2005). "Gradient plasticity theory with a variable length scale parameter." *Int. J. Solids Struct.*, 42(14), 3998–4029.
Zervos, A. (2008). "Finite elements for elasticity with microstructure and gradient elasticity." *Int. J. Numer. Methods Eng.*, 73(4), 564–595.
Zervos, A., Papanastasiou, P., and Vardoulakis, I. (2001a). "A finite element displacement formulation for gradient elastoplasticity." *Int. J. Numer. Methods Eng.*, 50(6), 1369–1388.
Zervos, A., Papanastasiou, P., and Vardoulakis, I. (2001b). "Modelling of localisation and scale effect in thick-walled cylinders with gradient elastoplasticity." *Int. J. Solids Struct.*, 38(30–31), 5081–5095.
Zervos, A., Papanastasiou, P., and Vardoulakis, I. (2008). "Shear localisation in thick-walled cylinders under internal pressure based on gradient elastoplasticity." *J. Theor. Appl. Mech.*, 38(1–2), 81–100.
Zervos, A., Vardoulakis, I., and Papanastasiou, P., (2007). "Influence of nonassociativity on localization and failure in geomechanics based on gradient elastoplasticity." *Int. J. Geomech.*, 7(1), 63–74.

J. Eng. Mech. 2009.135:203-213.